Hollow organosilica beads as reference particles for optical detection of extracellular vesicles

Zoltán Varga [*, †], Edwin van der Pol [‡, §, ¶], Marcell Pálmai [*], Raul Garcia-Diez [**,1], Christian Gollwitzer [**,2], Michael Krumrey [**], Jean-Luc Fraikin [††], Aleksandra Gasecka [§§,‡,¶], Najat Hajji [‡], Ton G. van Leeuwen [§,¶], Rienk Nieuwland [‡, ¶]

[*] Biological Nanochemistry Research Group, Institute of Materials and Environmental Chemistry, Research Centre for Natural Sciences, Hungarian Academy of Sciences, Budapest, Hungary

[†] Semmelweis University, Department of Biophysics and Radiation Biology, Budapest, Hungary

[‡] Laboratory of Experimental Clinical Chemistry, [§] Department of Biomedical Engineering and Physics and [¶] Vesicle Observation Center, Academic Medical Centre of the University of Amsterdam, Amsterdam, the Netherlands

[**] Physikalisch-Technische Bundesanstalt (PTB), Berlin, Germany

[††] Spectradyne LLC, Torrance CA, USA

[§§] 1st Chair and Department of Cardiology, Medical University of Warsaw, Warsaw, Poland

[1] Present address: Helmholtz-Zentrum Berlin für Materialien und Energie GmbH (HZB), Germany

[2] Present address: Bundesanstalt für Materialforschung und -prüfung (BAM), Berlin, Germany

Correspondence: Biological Nanochemistry Research Group, Institute of Materials and Environmental Chemistry, Research Centre for Natural Sciences, Hungarian Academy of Sciences, Magyar tudósok körútja 2, H-1117, Budapest, Hungary. Tel.: +36 1 382 6568 E-mail: varga.zoltan@ttk.mta.hu (Z. Varga)

Word count abstract: 243/250
Word count text: 3928/4000
No. of figures: 5
No. of references: 46

Running head: Hollow silica particles for vesicle detection

Keywords cell-derived microparticles, exosomes, extracellular vesicles, microvesicles, flow cytometry, microspheres

Essentials

- Standardization of extracellular vesicle (EV) measurements by flow cytometry needs improvement
- Hollow organosilica beads were prepared, characterized, and tested as reference particles
- Light scattering properties of hollow beads resemble that of platelet-derived EVs
- Hollow beads are ideal reference particles to standardize scatter flow cytometry research on EVs

Summary

Background: The concentration of extracellular vesicles (EVs) in body fluids is a promising biomarker for disease, and flow cytometry remains the clinically most applicable method to identify the cellular origin of single EVs in suspension. To compare concentration measurements of EVs between flow cytometers, solid polystyrene reference beads and EVs were distributed in the first ISTH organized inter-laboratory comparison studies. The beads were used to set size gates based on light scatter, and the concentration of EVs was measured within the size gates. However, polystyrene beads lead to false size determination of EVs due to the mismatch in refractive index between beads and EVs. Moreover, polystyrene beads gate different EV sizes on different flow cytometers. *Objective:* To prepare, characterize and test hollow organosilica beads (HOBs) as reference beads to set EV size gates in flow cytometry investigations. *Methods:* HOBs were prepared by a hard template sol-gel method and extensively characterized for morphology, size and colloidal stability. The applicability of HOBs as reference particles was investigated by flow cytometry using HOBs and platelet-derived EVs. *Results:* HOBs proved monodisperse with homogeneous shell thickness. Two angle light scattering measurements by flow cytometry confirmed that HOBs have light

scattering properties similar to platelet-derived EVs. *Conclusions:* Because HOBs resemble the structure and light scattering properties of EVs, HOBs with a given size will gate EVs of the same size. Therefore, HOBs are ideal reference beads to standardize optical measurements of the EV concentration within a predefined size range.

Introduction

Extracellular vesicles (EVs), including exosomes, microvesicles and other membrane surrounded structures released from cells, are in the forefront of biomedical research. Because EVs contribute to many physiological processes, EVs may serve as biomarkers for diseases, including cancer, neurological diseases, and thrombosis [1–4]. Despite the potential of EVs for diagnostic applications, gold standard techniques and reference materials for EV detection are lacking [5]. Detection of EVs is difficult because EVs are heterogeneous in size and composition, and most EVs are smaller than 500 nm [6–8]. Throughout this manuscript, size is defined as the diameter of the particle. Furthermore, the most widely studied body fluid with regard to EVs is blood, which contains not only EVs but similar-sized lipoprotein particles [9].

Because clinically relevant EVs are outnumbered by other EVs and lipoprotein particles, EVs are preferably characterized one by one. A recent international survey showed that optical methods are widely used to characterize single EVs [10]. Of all respondents who specified their single EV detection method, 80% used nanoparticle tracking analysis (NTA), 18% used tunable resistive pulse sensing (TRPS), and 29% used flow cytometry (bead capture assays excluded). Because only flow cytometry can identify single EVs at high throughput (>5,000 events/s) in a reproducible manner, flow cytometers hold most promise for clinical applications.

A flow cytometer detects light scattering and fluorescence of single particles in a hydrodynamically focused fluid stream. Because flow cytometers are designed to detect cells, which are much larger than EVs, commercially available flow cytometers do not detect all EVs. The detected concentration of EVs therefore strongly depends on the sensitivity of the flow cytometer, especially because the concentration of EVs increases with decreasing size [5]. To standardize flow cytometry measurements and enable data comparison, laboratories should detect the concentration of EVs within a well-defined size range. However, the arbitrary units of flow cytometry data preclude access to the EV size, thereby impeding standardization and comparison of measurement results.

The light scattering signals of two sizes of polystyrene beads are commonly used to gate EVs [11,12]. However, light scattering depends on the size, refractive index (RI), shape and structure of the particle, the RI of the medium, and the optical configuration of the flow cytometer. At a wavelength of 405 nm, which is used in modern flow cytometers to illuminate particles, polystyrene has an RI of 1.63 whereas EVs have an effective RI below 1.40 [13,14]. Due to this RI mismatch, 200 nm EVs scatters 40 to 300-fold less light than 200 nm polystyrene beads, as illustrated in Figure 1. Also 200 nm silica beads, which have an RI between 1.44 and 1.47, scatter 5 to 50-fold more light than similar-sized EVs [14–16]. Thus, the use of *solid* synthetic reference beads to standardize optical measurements of EVs leads to false size assignment.

Correct sizing of EVs by scattering flow cytometry requires reference particles with light scattering properties similar to EVs. EVs are concentric particles containing a ~4 nm phospholipid bilayer [6,17] with an RI of 1.46 ± 0.06 to 1.48 [18,19], surrounding an aqueous core with RI close to that of water (RI = 1.34 at a wavelength of 405 nm). The ideal reference particles are therefore stable, monodisperse, concentric particles with a high-RI shell and a low-RI core.

In this manuscript, we prepared, characterized and applied hollow organosilica beads (HOBs) with nominal sizes of 200 nm (HOB200) and 400 nm (HOB400) as reference materials for optical detection of EVs. Due to their concentric structure and organosilica shell, HOBs have an RI distribution resembling EVs. Based on Mie theory, HOBs are expected to have similar light scattering properties as EVs, as illustrated in Figure 1. The goals of this manuscript are to (1) determine the size distribution, concentration, structure, colloidal stability, and light scattering properties of the prepared HOBs, (2) confirm that HOBs have light scattering properties similar to EVs from blood plasma, and (3) use the HOBs to set a size gate that is independent of the collection angles of a flow cytometer.

Methods

Preparation of hollow organosilica beads (HOBs)

1,2-bis(triethoxysilyl)ethane (BTEE, 96%, Sigma-Aldrich, St. Louis, MO), cyclohexane (G.R., 99.99 %, Lach-Ner, Neratovice, Czech Republic), L-arginine (reagent grade, ≥98 %, TLC, Sigma-Aldrich) were used. Silica dispersions of 200 nm [PSI-0.2] and 400 nm [PSI-0.4]) in water were obtained from Kisker Biotech (Steinfurt, Germany). High purity deionized water (18.2 MΩ·cm) was used during synthesis.

HOBs were synthesized by combining a basic amino acid catalysis route with a hard template approach in a 4 mL glass vial [20,21]. Briefly, 2.6 mg of L-arginine and 300 µL of silica dispersion (50 mg mL^{-1}) serving as the template particles were added to 1.7 mL of water. Next, 130 µL of cyclohexane was overlayered on the aqueous phase and 134 µL of BTEE, the precursor of the organosilica shell, was injected into the non-polar phase. The reaction mixture was allowed to react under vigorous stirring (500 rpm) at 60 °C for 24 hours. Afterwards, cyclohexane was removed, the pH was adjusted to 12.75 ± 0.05 by adding 150

µL 1M NaOH solution and the dispersion was stirred for 24 hours at room temperature in order to etch the template silica core. The mesoporous shell structure and hydrolytic stability of organosilica under basic conditions enables etching of the silica core while maintaining the shell integrity. Finally, the sample was transferred into a 2 mL Slide-A-Lyzer™ MINI Dialysis Device (20K MWCO, Thermo Fisher Scientific, Waltham, MA) and dialysed against 42.5 mL of water for 4 times in 2 days to remove NaOH and side products.

Preparation and storage of cell-depleted plasma

Citrate-anticoagulated blood (0.32%) was collected from 10 healthy individuals [5 males and 5 females; age 45 ± 12 (mean ± standard deviation)] with informed consent by venipuncture without a tourniquet through a 21-gauge needle using a vacutainer system. To remove cells, blood was centrifuged twice (1,550 g, 20 minutes, 20˚C) using a Rotina 380 R centrifuge equipped with a swing-out rotor and a radius of 155 mm (Hettich Zentrifugen, Tuttlingen, Germany). The centrifugation parameters were 1,550 g for 20 minutes at 20˚C, acceleration speed 1, no brake. After a single centrifugation, plasma was transferred to a new 5 ml plastic tube, leaving ~1 cm plasma above the buffy layer. After the second centrifugation, plasma was collected and transferred carefully to a new 5 ml plastic tube, leaving ~100 µL at the bottom of the old tube. The number of remaining platelets after the second centrifugation is on average 0.5% of the initial platelet count in whole blood (n=4; data not shown), which is similar to the recommended ISTH protocol (2x 2,500 g for 15 minutes at 20˚C) [11]. Although our protocol and the ISTH protocol give similar results with regard to remaining platelets, we recommend to use the ISTH protocol to circumvent confusion and to enable the comparison of results between studies and laboratories [22]. Aliquots of 100 µL cell-depleted plasma were snap-frozen in liquid nitrogen for 15 minutes and stored at -80 °C until use.

After thawing on ice, 20 µL of plasma was incubated in the dark for 120 minutes at 20 °C with 2.5 µL phycoerythrin (PE)-conjugated CD61 or IgG1-PE control (555754 and 340013, respectively; both 6.25 µg/ mL, Becton Dickinson, CA). Labeling was stopped by addition of 200 µL, 50 nm filtered (Whatman, Maidstone, UK), citrate-containing (0.32%) phosphate buffered saline (PBS; pH 7.4). To verify the presence of EVs, cell-depleted plasma was characterized by NTA and TEM (Details in Supplementary Information).

Transmission electron microscopy (TEM)

Morphological investigations of HOBs were carried out on a MORGAGNI 268D (FEI, Eindhoven, Netherlands) transmission electron microscope. Diluted sample was dropped and dried on a carbon coated copper grid. The supplementary information contains the TEM protocol for EVs from cell-depleted plasma.

Dynamic light scattering (DLS)

HOBs were characterized by DLS (W130i Dynamic Light Scattering System, AvidNano, High Wycombe, UK). Samples were diluted 50-fold with ultrapure water (Merck Millipore, Billerica, MA). Low volume disposable plastic cuvette was used for the DLS measurements (UVette, Eppendorf Austria GmbH, Austria), and data evaluation was performed using the iSize 3.0 software (AvidNano) utilizing the CONTIN algorithm.

Small-angle X-ray scattering (SAXS)

HOBs were characterized by SAXS at the four-crystal monochromator beamline of PTB [23,24] at the synchrotron radiation facility BESSY II (Helmholtz-Zentrum Berlin, Germany). The mean size, size distribution, and shell thickness of HOBs were determined by using a least-squares fitting of a model function to the experimentally measured scattering curves (details in Supplementary Information) [25,26].

Zeta potential

Zeta potential measurements of HOBs were performed by using a Malvern Zetasizer Nano ZS (Malvern, Worcestershire, UK) equipped with He-Ne laser (λ = 633 nm) and backscatter detector at fixed angle of 173°.

Nanoparticle tracking analysis (NTA)

A dark-field microscope (NS500; Nanosight, Amesbury, UK) with a 45-mW 405-nm laser and an electron multiplying charge-coupled device was used to determine the size and concentration of HOBs by NTA. Samples were diluted 10,000-fold (HOB200) or 100-fold (HOB400) in 50 nm filtered (Whatman) de-ionized water. Per sample, 30 videos of 10 s were captured at 22.0 °C using camera level 15 (HOB200) or 12 (HOB400) [22]. Data were analysed by NTA 3.1 Build 3.1.54 (Nanosight), assuming a medium viscosity of 0.95 cP and using a threshold of 10 gray values. The supplementary information contains the NTA protocol for EVs from cell-depleted plasma.

Tunable resistive pulse sensing (TRPS)

TRPS (qNano, Izon Science, Oxford, UK) was used to determine the size and concentration of HOBs. Samples were diluted 500-fold (HOB200) or 50-fold (HOB400) in 50 nm filtered (Whatman) PBS. HOBs were measured with NP200 (HOB200) and NP400 (HOB400) nanopores. The voltage was adjusted between 0.40 and 0.70 V to obtain a baseline current of 125 nA using a nanopore stretch of 47.00 mm [27]. Next, the stretch was adjusted such that the amplitude of the resistive pulses of reference beads (Izon Science) is within the range recommended by the manufacturer. This resulted in a stretch between 45.50 and 47.00 mm. Finally, the voltage was adjusted between 0.40 and 0.70 V to get the baseline current as close as possible to 125 nA. Samples were measured with an external pressure of 7.0 mbar and at least 1,000 beads per sample were analyzed. Particle size and concentration were calibrated with reference beads (Izon Science). Data acquisition and processing were done with Izon control suite version 3.2.2.268.

Microfluidic resistive pulse sensing (MRPS)

MRPS (nCS1, Spectradyne LLC, Torrance, CA) was used to determine the size and concentration of HOBs [28]. Samples were diluted 1,000-fold (HOB200) or 100-fold (HOB400) in 50 nm filtered (Whatman) PBS containing 0.6 mM sodium dodecyl sulfate. All samples were measured with a TS-900 cartridge at a voltage of 4 V. To relate the frequency of resistive pulses to the particle concentration, 695 nm reference beads (Spectradyne) with a concentration of $2 \cdot 10^8$ mL^{-1} were used.

Flow cytometry

A flow cytometer (A60-Micro; Apogee, Hemel Hempstead, UK) equipped with a 200 mW 405 nm laser was used to detect forward scattered light (FSC), side scattered light (SSC) and fluorescence of beads and EVs. SSC was used as the trigger channel with the threshold at 14 arbitrary units. For the FSC, SSC and PE fluorescence channel, the gain was 1 and the voltages were 380 V, 375 V, and 520 V, respectively. Samples were measured for 1 minute at a flow rate of 3.01 µL/minute and with a sheath pressure of 150 mbar. Rosetta Calibration (Exometry, Amsterdam, The Netherlands) was used to relate side scatter to the size and RI of nanoparticles by Mie theory [29]. To validate this relation, side scatter of silica beads (Kisker Biotech, Steinfurt, Germany) was measured at a concentration of 10^7 mL^{-1}. Median fluorescent intensity was related to molecules of equivalent soluble fluorochrome (MESF) for phycoerythin (PE) using the SPHERO PE Calibration kit (ECFP-F2-5K, Spherotech). Figure S3 shows the relation between the measured PE intensity in arbitrary units and MESF, which was obtained by least square fitting the logarithm of the data. The gate of the PE channel was set at 51 MESF. HOB200 and HOB400 were diluted 10^5-fold and 10^3-fold in purified water to a detected concentration of $6.7 \cdot 10^6$ mL^{-1} and $1.4 \cdot 10^7$ mL^{-1}, respectively. Cell-depleted plasma was diluted 66-fold in PBS to avoid swarm detection, as confirmed by serial dilutions [30]. For the cell-depleted plasma, data of 5 measurements were combined to create the scatter plot shown in Fig. 5. Data acquisition was done with Apogee software and processed using FlowJo v.10.3 (FlowJo LLC, Ashland, OR).

Results

Size distribution of HOBs

The prepared HOBs were characterized by TEM, NTA, TRPS, MRPS, DLS and SAXS. TEM images show that HOBs have homogeneous morphology and uniform layer thicknesses (Figure 2). Figure 3 shows the size distributions of HOBs obtained by the single particle detection methods TEM, NTA, TRPS, and MRPS. Among ensemble techniques, DLS resulted mean sizes of 188 nm and 356 nm, and full-width-at-half-maximum (FWHM) values of 52 nm and 118 nm for HOB200 and HOB400, respectively. SAXS, which is the only traceable method used in this study, resulted in mean sizes (value ± uncertainty) of 189±2 nm and 374±10 nm for HOB200 and HOB400, respectively. SAXS obtained a polydispersity (FWHM/mean) below 15%. Table S1 shows a summary of all size measurements.

Concentration, structure and stability of HOBs

NTA, TRPS, MRPS and flow cytometry measured concentrations of $2.2 \cdot 10^{12}$, $2.0 \cdot 10^{11}$, $2.7 \cdot 10^{11}$, and $6.7 \cdot 10^{11}$ particles/ml for HOB200 and $4.4 \cdot 10^{10}$, $1.6 \cdot 10^{10}$, $1.4 \cdot 10^{10}$ and $1.4 \cdot 10^{10}$ particles/ml for HOB400, respectively.

Besides size, SAXS also provides information on the structure and electron density distribution of HOBs. By fitting a core-shell model to the measured scattering curves we obtained a shell thickness of (8.1 ± 0.5) nm for HOB200 and (6.4 ± 0.7) nm for HOB400. Furthermore, we obtained an average electron density of the core of 345 nm^{-3} for both samples, which is close to the electron density of water (333 nm^{-3}). This observation confirms the successful etching of the template silica core.

The colloidal stability of the HOBs, which describes the aggregation properties of the beads, was evaluated by Zeta potential measurements. We found highly negative zeta

potentials (-56.6 mV for HOB200 and -58.1 mV for HOB400), which we associate to the dissociation of surface silanol groups [31]. The highly negative zeta potentials suggest that HOBs exhibit excellent colloidal stability in water at pH 7.4.

Light scattering properties of HOBs measured by flow cytometry

To test the applicability of HOBs as reference particles for characterization of EVs by flow cytometry, we compared light scattering properties of HOBs and EVs. Figure 4 (a) shows the side scattering intensity of polystyrene beads, silica beads, and HOBs measured by flow cytometry and calculated by Mie theory. Whereas the polystyrene (coefficient of determination, R^2=1.00) and silica beads (R^2=0.97) are well-described by a solid sphere Mie model, the HOBs (R^2=0.95) are well-described by a hollow sphere Mie model. By least square fitting the theory to the data, we obtained a shell thickness of 10.1 nm for the HOBs, which is close to the shell thickness determined by SAXS. Due to the hollow structure, HOBs scatter at least an order of magnitude less light than similar-sized solid silica beads. The scattering intensity of HOBs thereby overlaps with the scattering intensity expected from EVs. We modelled EVs as concentric particles with a 4 nm shell (RI = 1.48) [32–36] and a core ($1.35 \leq RI \leq 1.37$) [37–40]. The RI range of the core corresponds to a realistic protein concentration between 10% and 20% [41]. Our model parameters result in scattering intensities similar to platelet-derived EVs with a median RI of 1.37 and a mode RI of 1.39 at 405 nm, which was previously measured under the assumption that EVs have a homogeneous RI distribution [13,42]. More accurate estimates of the RI distribution of EVs require monodisperse EV populations, which are hitherto unavailable.

To demonstrate that HOBs have light scattering properties similar to EVs, Fig. 4 (b) shows the measured side scatter (SSC) intensity versus forward scatter (FSC) intensity for HOBs, platelet-derived (CD61+) EVs from cell-depleted plasma, and, for comparison, 125 nm polystyrene beads and 182 nm and 402 nm silica beads. As a reference, the arrows relate

the size range of EVs expected from Mie theory to their FSC and SSC values. The data show that for a given FSC of this flow cytometer, HOBs have low SSC whereas polystyrene and silica beads have high SSC compared to EVs. However, HOBs are within the theoretical EV size range and are therefore expected to be better reference materials to standardize flow cytometry measurements on EVs.

HOBs outperform solid beads to standardize EV flow cytometry

To demonstrate that HOBs can be used to determine the EV concentration independent of the light scattering collection angles of a flow cytometer, we determined the concentration of platelet-derived EVs using the FSC or SSC detector within size gates set by HOBs. Because the sensitivity and the scatter to size relationship differ between the FSC and SSC detectors of our flow cytometer [5], while the flow rate and sample composition are the same for both detectors, this experiment may demonstrate that HOBs set an EV size gate independent of the collection angles. Fig. 5 shows the concentration of platelet-derived EVs within gates set by polystyrene beads, silica beads, and HOBs for the FSC and SSC detector. Figure S4 shows the applied gates at FSC versus SSC scatter plots. The percentage difference in the gated concentration relative to the mean concentration is smallest for the gates set by HOBs compared to solid beads, suggesting that HOBs outperform solid beads to standardize EV flow cytometry.

Discussion

Standardization of flow cytometry measurements is essential to explore the diagnostic potential of EVs. Since the scattering intensities measured by flow cytometry are in arbitrary units, there is a need for reference beads with known size and light scattering properties

similar to those of EVs. The optical properties of a particle depend not only on the size, but also on the RI distribution within the particle. EVs typically have a 4 nm thick shell of high RI and a core of low RI. In contrast, polystyrene and silica beads consist of a homogeneously distributed high RI material and therefore scatter orders of magnitude more light than similar-sized EVs (Fig. 4a). In this manuscript, we introduce HOBs with similar light scattering properties as EVs to standardize optical measurements on EVs.

HOBs with smooth surfaces were produced by optimizing the existing hard template approach proposed by Koike et al. [20]. All established particle measurement methods (TEM, NTA, TRPS, SAXS) confirmed a narrow size distribution (FWHM/MEAN < 0.25) of HOBs. The relative standard deviation of the mean size values obtained by the different methods is below 10%, which indicate good agreement between used methods. All methods indicate the presence of contaminants, which are smaller than and have a lower concentration than HOBs. These contaminants might originate from incomplete particles or from the polycondensation of the organosilica precursor. Introducing a further purification step during the synthesis may eliminate these contaminants.

The hollow core-shell structure of the prepared HOBs was confirmed by TEM and SAXS, and indirectly by flow cytometry. NTA, TRPS, MRPS and flow cytometry were further used to determine the concentrations of the prepared HOBs. The obtained values show an order of magnitude deviation for the HOB200 and a factor of 3.4 deviation for HOB400. However, concentration measurements require careful interpretation, especially because no standards or primary methods exist and no certified reference materials are available for the concentration determination of nanoparticles [43].

Flow cytometry measurements show that HOBs scatter approximately an order of magnitude less light than similar sized solid silica beads (Fig. 4a). The measured light scatter of HOBs thereby overlaps with the expected light scatter for EVs, which is also expected

344 based on the spatial RI distribution within both particle types. To demonstrate that HOBs and
345 EVs indeed have similar light scattering properties, we measured the FSC and SSC of HOBs
346 and platelet-derived EVs from blood plasma (Fig. 4b). We found that HOBs have a low SSC
347 (or high FSC) whereas polystyrene and silica beads have high SSC (or low FSC) compared to
348 EVs. However, the shell thickness of HOBs can in principle be tuned to exactly match the
349 FSC and SSC properties of EVs. Moreover, HOBs are closer to the theoretical EV size, which
350 emphasizes the wrong size assignment of EVs when solid reference beads are used to set
351 gates. For example, 182 nm solid silica beads produce comparable SSC and FSC signals to
352 374 nm HOBs, meaning that a 2-fold difference in size assignment between solid and hollow
353 silica beads exists.
354 As proof of the pudding, we applied HOBs to set size gates on FSC and SSC, which
355 collect light over different collection angles, resulting in totally different scatter to size
356 relations [5]. Fig. 5 shows that the variation in the gated EV concentration of these detectors
357 was minimal for gates set by HOBs, confirming that HOBs have similar optical properties to
358 EVs and in fact define an EV gate in nanometers. A multicenter and multi flow cytometer
359 follow-up study is required to demonstrate the superiority of HOBs over solid beads.
360 The illumination wavelength of our flow cytometer is 405 nm. We expect that EV size
361 gates set by HOBs are also applicable to flow cytometers with other common illumination
362 wavelengths, such as 375 nm and 488 nm. The refractive indices of glass and water at 375 nm
363 are almost 0.01 higher than the refractive indices of glass and water at 488 nm. However,
364 scattering depends on the RI contrast, in this case between water and the shell of the HOBs or
365 EVs. Because within this wavelength range the dispersion relations of glass and water have
366 similar slopes, the RI contrast between water and glass remains similar at 375 nm and 488 nm
367 [44,45]. The dispersion relation of the shell of EVs is unknown, but based on the dispersion

relations of organic materials, negligible changes in the RI contrast between water and the shell of EVs is expected between 375 nm and 488 nm.

An alternative to setting EV size gates with HOBs, is to relate the scattering intensity of solid polystyrene and silica reference beads to that of EVs by Mie theory [29]. Mie theory accounts for RI differences, but requires complex software and knowledge of the optical configuration of the flow cytometer. HOBs are more practical in use because HOBs can directly be used to set an EV size gate in nanometers, due to the almost similar light scattering properties of EVs and HOBs. Perhaps the best solution would be the use of Mie theory in combination with HOBs to allow the user flexibility in selection of an EV size gate by flow cytometry.

Conclusions

In summary, we introduced HOBs to be used as reference beads for optical characterization of EVs. Thorough characterization of the prepared HOBs revealed narrow size distributions, colloidal stability, and homogeneous hollow core-shell structure of HOBs. Compared to potential biological reference particles [46], which like HOBs resemble the light scattering properties of EVs, safety, monodispersity and stability of HOBs are superior. The performed flow cytometry investigations confirm that HOBs have similar light scattering properties as EVs and therefore are more suitable as reference beads for flow cytometry characterization of EVs than solid polystyrene or silica beads. HOBs can be used to set size gates in nanometers independent from the optical configuration of a flow cytometer. Therefore, HOBs are ideal reference beads to standardize optical measurements of the EV concentration within a predefined size range, which may facilitate the comparison of EV measurements between instruments and institutes.

Addendum

Z. Varga and E. van der Pol designed and performed the research and wrote the paper; M. Pálmai contributed to the synthesis and characterization; R. Garcia-Diez, C. Gollwitzer, and M. Krumrey performed the SAXS analysis and contributed to writing the paper; J-L. Fraikin performed MRPS analysis, A. Gasecka and N. Hajji contributed to characterization; T. G. van Leeuwen contributed to writing the paper; R. Nieuwland designed the research and contributed to writing the paper.

Acknowledgements

We thank Chi Hau and Linda Rikkert (Laboratory of Experimental Clinical Chemistry, Academic Medical Center , University of Amsterdam, Amsterdam, The Netherlands) for the TEM investigation of the cell-depleted plasma sample. This work was supported by the National Research, Development and Innovation Office (Hungary) under grant numbers PD 121326 and NVKP_16-1-2016-0007. ZV was supported by the János Bolyai Research Fellowship of the Hungarian Academy of Sciences. Part of this work was supported by the Cancer-ID program (www.utwente.nl/tnw/cancer-id), the MEMPHISII program of the Netherlands Technology Foundation STW, and the VENI program (15924, Edwin van der Pol) of the Netherlands Organisation for Scientific Research - Domain Applied and Engineering Sciences (NWO-TTW).

Disclosure of Conflict of Interest

E. van der Pol is co-founder and shareholder of Exometry B.V. The authors declare no further competing financial interests.

Supporting Information

Additional Supporting Information may be found in the online version of this article:

Fig. S1. NTA and TEM characterization of cell-depleted plasma

Table S1. Summary of size distribution parameters of HOBs

Data S1. Details of the SAXS analysis of HOBs.

Fig. S2. SAXS curves of HOBs.

Fig. S3. MESF calibration of Phycoerythrin (PE) channel.

Fig. S4. Flow cytometry data of extracellular vesicles from plasma

References

1 van Eijndhoven MAJ, Zijlstra JM, Groenewegen NJ, Drees EEE, van Niele S, Baglio SR, Koppers-Lalic D, van der Voorn H, Libregts SFWM, Wauben MHM, de Menezes RX, van Weering JRT, Nieuwland R, Visser L, van den Berg A, de Jong D, Pegtel DM. Plasma vesicle miRNAs for therapy response monitoring in Hodgkin lymphoma patients. *JCI Insight* 2016; **1**: e89631.

2 Hoshino A, Costa-Silva B, Shen T-L, Rodrigues G, Hashimoto A, Tesic Mark M, Molina H, Kohsaka S, Di Giannatale A, Ceder S, Singh S, Williams C, Soplop N, Uryu K, Pharmer L, King T, Bojmar L, Davies AE, Ararso Y, Zhang T, et al. Tumour exosome integrins determine organotropic metastasis. *Nature* 2015; **527**: 329–35.

3 Melo SA, Luecke LB, Kahlert C, Fernandez AF, Gammon ST, Kaye J, LeBleu VS, Mittendorf EA, Weitz J, Rahbari N, Reissfelder C, Pilarsky C, Fraga MF, Piwnica-Worms D, Kalluri R. Glypican-1 identifies cancer exosomes and detects early pancreatic cancer. *Nature* 2015; **523**: 177–82.

4 van der Pol E, Böing AN, Gool EL, Nieuwland R. Recent developments in the nomenclature, presence, isolation, detection and clinical impact of extracellular vesicles. *J Thromb Haemost JTH* 2016; **14**: 48–56.

5 van der Pol E, Coumans F a. W, Grootemaat AE, Gardiner C, Sargent IL, Harrison P, Sturk A, van Leeuwen TG, Nieuwland R. Particle size distribution of exosomes and microvesicles determined by transmission electron microscopy, flow cytometry, nanoparticle tracking analysis, and resistive pulse sensing. *J Thromb Haemost JTH* 2014; **12**: 1182–92.

6 Arraud N, Linares R, Tan S, Gounou C, Pasquet J-M, Mornet S, Brisson AR. Extracellular vesicles from blood plasma: determination of their morphology, size, phenotype and concentration. *J Thromb Haemost JTH* 2014; **12**: 614–27.

7 Brisson AR, Tan S, Linares R, Gounou C, Arraud N. Extracellular vesicles from activated platelets: a semiquantitative cryo-electron microscopy and immuno-gold labeling study. *Platelets* 2017; **28**: 263–71.

8 Varga Z, Yuana Y, Grootemaat AE, van der Pol E, Gollwitzer C, Krumrey M, Nieuwland R. Towards traceable size determination of extracellular vesicles. *J Extracell Vesicles* 2014; **3**.

9 Sódar BW, Kittel Á, Pálóczi K, Vukman KV, Osteikoetxea X, Szabó-Taylor K, Németh A, Sperlágh B, Baranyai T, Giricz Z, Wiener Z, Turiák L, Drahos L, Pállinger É, Vékey K, Ferdinandy P, Falus A, Buzás EI. Low-density lipoprotein mimics blood plasma-derived exosomes and microvesicles during isolation and detection. *Sci Rep* 2016; **6**: 24316.

10 Gardiner C, Di Vizio D, Sahoo S, Théry C, Witwer KW, Wauben M, Hill AF. Techniques used for the isolation and characterization of extracellular vesicles: results of a worldwide survey. *J Extracell Vesicles* 2016; **5**: 32945.

11 Lacroix R, Robert S, Poncelet P, Kasthuri RS, Key NS, Dignat-George F, ISTH SSC Workshop. Standardization of platelet-derived microparticle enumeration by flow cytometry with calibrated beads: results of the International Society on Thrombosis and Haemostasis SSC Collaborative workshop. *J Thromb Haemost JTH* 2010; **8**: 2571–4.

12 Cointe S, Judicone C, Robert S, Mooberry MJ, Poncelet P, Wauben M, Nieuwland R, Key NS, Dignat-George F, Lacroix R. Standardization of microparticle enumeration across different flow cytometry platforms: results of a multicenter collaborative workshop. *J Thromb Haemost JTH* 2017; **15**: 187–93.

13 Gardiner C, Shaw M, Hole P, Smith J, Tannetta D, Redman CW, Sargent IL. Measurement of refractive index by nanoparticle tracking analysis reveals heterogeneity in extracellular vesicles. *J Extracell Vesicles* 2014; **3**: 25361.

14 van der Pol E, Coumans FA, Sturk A, Nieuwland R, van Leeuwen TG. Refractive index determination of nanoparticles in suspension using nanoparticle tracking analysis. *Nano Lett* 2014; **14**: 6195–201.

15 Parida BK, Garrastazu H, Aden JK, Cap AP, McFaul SJ. Silica microspheres are superior to polystyrene for microvesicle analysis by flow cytometry. *Thromb Res* 2015; **135**: 1000–6.

16 Chandler WL, Yeung W, Tait JF. A new microparticle size calibration standard for use in measuring smaller microparticles using a new flow cytometer. *J Thromb Haemost JTH* 2011; **9**: 1216–24.

17 Issman L, Brenner B, Talmon Y, Aharon A. Cryogenic transmission electron microscopy nanostructural study of shed microparticles. *PLoS One* 2013; **8**: e83680.

18 van Manen H-J, Verkuijlen P, Wittendorp P, Subramaniam V, van den Berg TK, Roos D, Otto C. Refractive index sensing of green fluorescent proteins in living cells using

fluorescence lifetime imaging microscopy. *Biophys J* 2008; **94**: L67-69.

19 Beuthan J, Minet O, Helfmann J, Herrig M, Müller G. The spatial variation of the refractive index in biological cells. *Phys Med Biol* 1996; **41**: 369–82.

20 Koike N, Ikuno T, Okubo T, Shimojima A. Synthesis of monodisperse organosilica nanoparticles with hollow interiors and porous shells using silica nanospheres as templates. *Chem Commun* 2013; **49**: 4998–5000.

21 Hartlen KD, Athanasopoulos APT, Kitaev V. Facile Preparation of Highly Monodisperse Small Silica Spheres (15 to >200 nm) Suitable for Colloidal Templating and Formation of Ordered Arrays. *Langmuir* 2008; **24**: 1714–20.

22 Coumans FAW, Brisson AR, Buzas EI, Dignat-George F, Drees EEE, El-Andaloussi S, Emanueli C, Gasecka A, Hendrix A, Hill AF, Lacroix R, Lee Y, van Leeuwen TG, Mackman N, Mäger I, Nolan JP, van der Pol E, Pegtel DM, Sahoo S, Siljander PRM, et al. Methodological Guidelines to Study Extracellular Vesicles. *Circ Res* 2017; **120**: 1632–48.

23 Krumrey M, Ulm G. High-accuracy detector calibration at the PTB four-crystal monochromator beamline. *Nucl Instrum Methods Phys Res Sect Accel Spectrometers Detect Assoc Equip* 2001; **467**: 1175–8.

24 Gleber G, Cibik L, Haas S, Hoell A, Müller P, Krumrey M. Traceable size determination of PMMA nanoparticles based on Small Angle X-ray Scattering (SAXS). *J Phys Conf Ser* 2010; **247**: 012027.

25 Varga Z, Yuana Y, Grootemaat AE, van der Pol E, Gollwitzer C, Krumrey M, Nieuwland R. Towards traceable size determination of extracellular vesicles. *J Extracell Vesicles* 2014; **3**: 23298.

26 van der Pol E, Coumans F, Varga Z, Krumrey M, Nieuwland R. Innovation in detection of microparticles and exosomes. *J Thromb Haemost* 2013; **11**: 36–45.

27 Coumans FAW, van der Pol E, Böing AN, Hajji N, Sturk G, van Leeuwen TG, Nieuwland R. Reproducible extracellular vesicle size and concentration determination with tunable resistive pulse sensing. *J Extracell Vesicles* 2014; **3**: 25922.

28 Fraikin J-L, Teesalu T, McKenney CM, Ruoslahti E, Cleland AN. A high-throughput label-free nanoparticle analyser. *Nat Nanotechnol* 2011; **6**: 308–13.

29 van der Pol E, ISTH-SSC-VB Working group, Hau C, Sturk A, van Leeuwen TG, Nieuwland R, Coumans FAW. Standardization of extracellular vesicle measurements by flow cytometry through vesicle diameter approximation. *J Thromb Haemost* : (submitted).

30 de Rond L, van der Pol E, Hau CM, Varga Z, Sturk A, van Leeuwen TG, Nieuwland R, Coumans FAW. Comparison of Generic Fluorescent Markers for Detection of Extracellular Vesicles by Flow Cytometry. *Clin Chem* 2018; .

31 Pálmai M, Nagy LN, Mihály J, Varga Z, Tárkányi G, Mizsei R, Szigyártó IC, Kiss T,

523 Kremmer T, Bóta A. Preparation, purification, and characterization of aminopropyl-
524 functionalized silica sol. *J Colloid Interface Sci* 2013; **390**: 34–40.

525 32 Mitra K, Ubarretxena-Belandia I, Taguchi T, Warren G, Engelman DM. Modulation
526 of the bilayer thickness of exocytic pathway membranes by membrane proteins rather than
527 cholesterol. *Proc Natl Acad Sci U S A* 2004; **101**: 4083–8.

528 33 Lewis BA, Engelman DM. Lipid bilayer thickness varies linearly with acyl chain
529 length in fluid phosphatidylcholine vesicles. *J Mol Biol* 1983; **166**: 211–7.

530 34 Balgavý P, Dubnicková M, Kucerka N, Kiselev MA, Yaradaikin SP, Uhríková D.
531 Bilayer thickness and lipid interface area in unilamellar extruded 1,2-
532 diacylphosphatidylcholine liposomes: a small-angle neutron scattering study. *Biochim*
533 *Biophys Acta* 2001; **1512**: 40–52.

534 35 Tahara Y, Fujiyoshi Y. A new method to measure bilayer thickness: cryo-electron
535 microscopy of frozen hydrated liposomes and image simulation. *Micron Oxf Engl 1993* 1994;
536 **25**: 141–9.

537 36 Lambert O, Gerke V, Bader MF, Porte F, Brisson A. Structural analysis of junctions
538 formed between lipid membranes and several annexins by cryo-electron microscopy. *J Mol*
539 *Biol* 1997; **272**: 42–55.

540 37 Horváth R, Fricsovszky G, Papp E. Application of the optical waveguide lightmode
541 spectroscopy to monitor lipid bilayer phase transition. *Biosens Bioelectron* 2003; **18**: 415–28.

542 38 Ducharme D, Max JJ, Salesse C, Leblanc RM. Ellipsometric study of the physical
543 states of phosphatidylcholines at the air-water interface. *J Phys Chem* 1990; **94**: 1925–32.

544 39 Mashaghi A, Swann M, Popplewell J, Textor M, Reimhult E. Optical anisotropy of
545 supported lipid structures probed by waveguide spectroscopy and its application to study of
546 supported lipid bilayer formation kinetics. *Anal Chem* 2008; **80**: 3666–76.

547 40 Kienle DF, de Souza JV, Watkins EB, Kuhl TL. Thickness and refractive index of
548 DPPC and DPPE monolayers by multiple-beam interferometry. *Anal Bioanal Chem* 2014;
549 **406**: 4725–33.

550 41 Barer R, Joseph S. Refractometry of living cells: Part I. Basic principles. *J Cell Sci*
551 1954; **3**: 399–423.

552 42 van der Pol E, de Rond L, Coumans FAW, Gool EL, Böing AN, Sturk A, Nieuwland
553 R, van Leeuwen TG. Absolute sizing and label-free identification of extracellular vesicles by
554 flow cytometry. *Nanomedicine Nanotechnol Biol Med* 2018; **14**: 801–10.

555 43 Shang J, Gao X. Nanoparticle counting: towards accurate determination of the molar
556 concentration. *Chem Soc Rev* 2014; **43**: 7267–78.

557 44 Handbook of Optics, 3rd edition, Vol. 4. McGraw-Hill; 2009.

45 Daimon M, Masumura A. Measurement of the refractive index of distilled water from the near-infrared region to the ultraviolet region. *Appl Opt* 2007; **46**: 3811–20.

46 Valkonen S, van der Pol E, Böing A, Yuana Y, Yliperttula M, Nieuwland R, Laitinen S, Siljander PRM. Biological reference materials for extracellular vesicle studies. *Eur J Pharm Sci Off J Eur Fed Pharm Sci* 2017; **98**: 4–16.

Figures

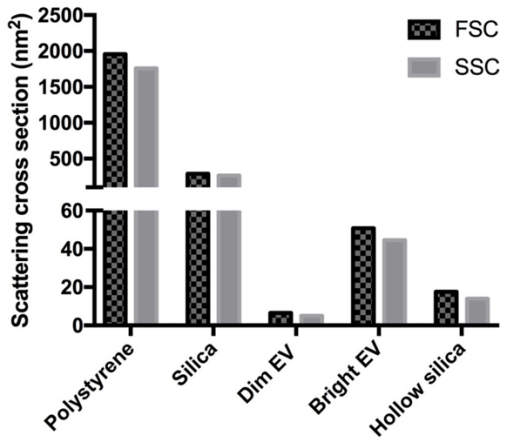

Figure 1 Theoretical forward and side scattering cross sections (FSC and SSC, respectively) of polystyrene beads, silica beads, dim and bright extracellular vesicles (EVs), and hollow organosilica beads (HOB) for an Apogee A60-Micro flow cytometer. The model calculations were performed using the Mie scattering theory. The following refractive indices at a wavelength of 405 nm were used for the calculations: 1.63 for polystyrene, 1.46 for silica, 1.48 for the EV shell, 1.34 for core of dim EV, 1.38 for the core of bright EV, 1.46 for the HOB shell, and 1.34 for the HOB core. The particle size (diameter) was 200 nm in all cases, and the shell thickness was set to 5 nm for EVs and 10 nm for HOBs.

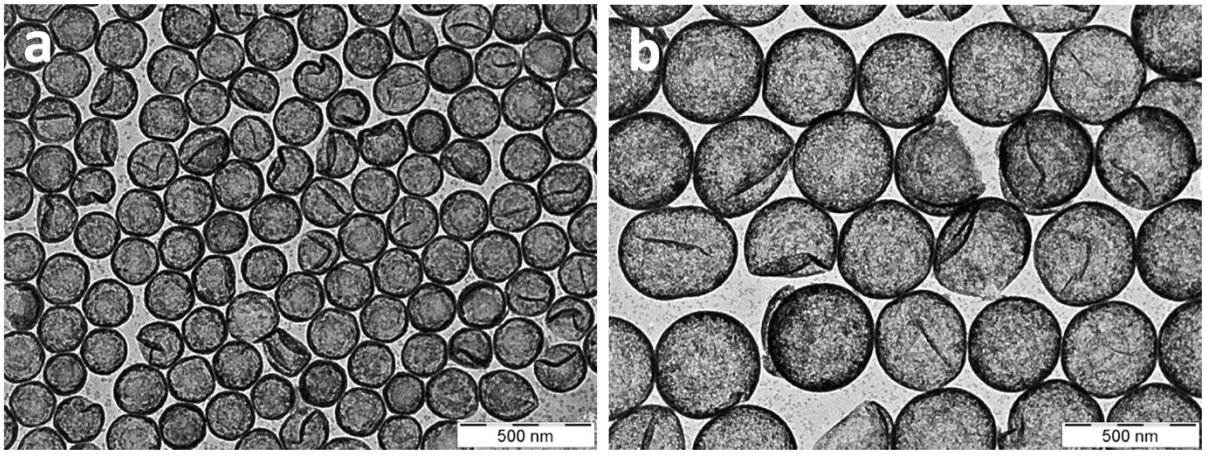

Figure 2 Transmission electron microscopy (TEM) analysis of hollow organosilica beads (HOBs) prepared by using nominal 200 nm (a) and 400 nm (b) sized silica templates.

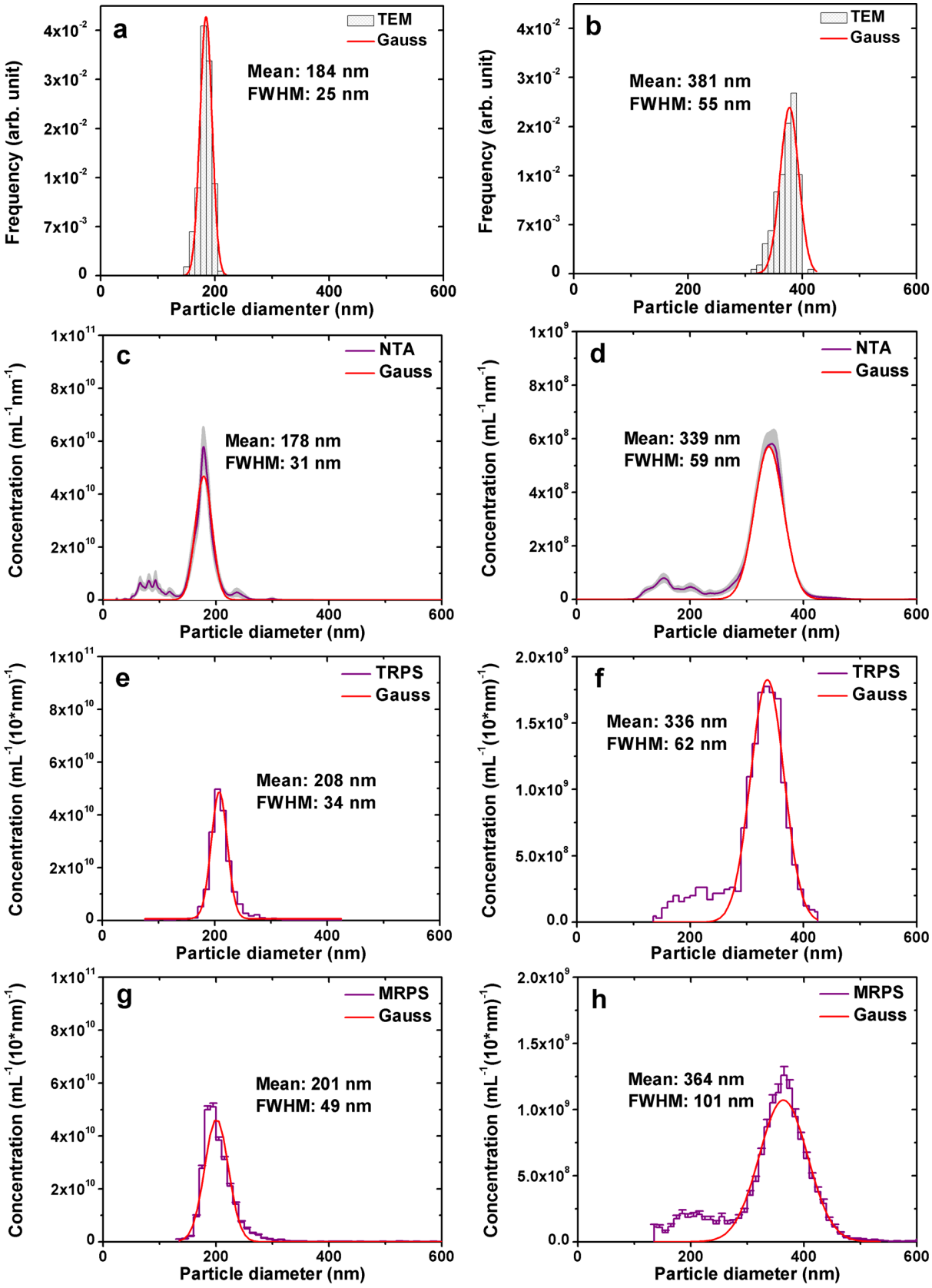

Figure 3. Size (diameter) distributions of nominal 200 nm and 400 nm sized hollow organosilica beads (HOBs) by single particle detection methods: transmission electron

microscopy (TEM; a, b; 10 nm bin width), particle tracking analysis (NTA; c, d; 1 nm bin width; the grey area represents the standard deviation), tunable resistive pulse sensing (TRPS; e, f; 10 nm bin width) and microfluidic resistive pulse sensing (MRPS; g, h; the error bars represents the standard deviation, 10 nm bin width). Mean sizes and full-width-at-half-maximum values from Gaussian fits of the distributions are indicated for each method. In case of HOB400, a shoulder can be seen on the distributions which might be attributed to incomplete particles or polycondensation of the organosilica precursor during the synthesis.

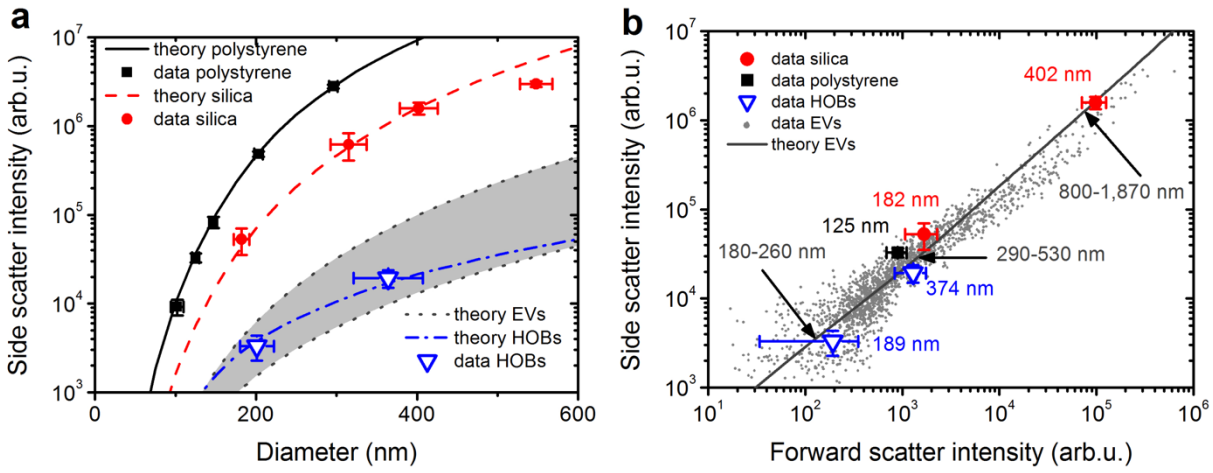

Figure 4 Light scattering properties of polystyrene beads (squares), silica beads (circles), hollow organosilica beads (HOBs; triangles), and platelet-derived (CD61+) extracellular vesicles (EVs; dots) from human plasma measured (symbols) by flow cytometry and calculated (lines) by Mie theory. (a) Side scatter versus size (diameter). Whereas polystyrene and silica beads scatter orders of magnitudes more light than similar-sized EVs, HOBs resemble the expected side scatter properties of EVs (gray area). (b) Side scatter versus forward scatter. In contrast to polystyrene and silica beads, HOBs have forward and side scatter intensities similar to EVs of the same size. Data points and error bars represent the mean and standard deviation, respectively. The arrows relate the size range of EVs expected from Mie theory to their FSC and SSC values. Size ranges are based on the SSC confidence interval (gray area) for EVs in (a). The following refractive indices at a wavelength of 405 nm

were used for the calculations: 1.63 for polystyrene, 1.46 for silica, 1.48 for the EV shell, 1.35 and 1.37 for the EV core to obtain the lower and upper boundary of the grey area in (a), respectively, 1.36 for the EV core in (b), 1.48 for the HOB shell, and 1.34 for the water. Least square fitting resulted in a shell thickness of 10.1 nm for the HOBs.

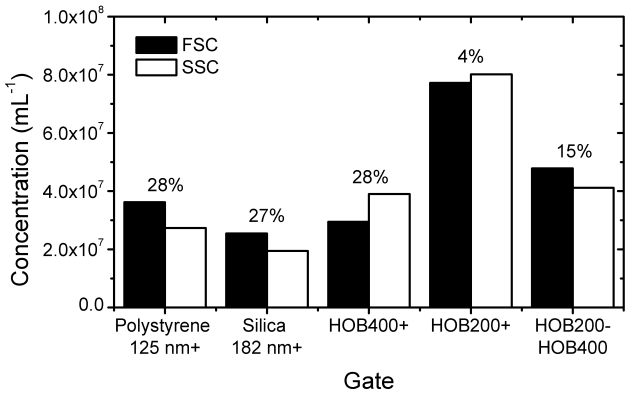

Figure 5. Concentration of platelet-derived extracellular vesicles (EVs) within gates set by polystyrene beads, silica beads, and hollow organosilica beads (HOBs) for the forward scattered light (FSC) and side scattered light (SSC) detector. Concentrations are corrected for sample dilutions. For the first 4 gates, the indicated bead is used as the lower size gate and no upper size gate is applied. For the HOB200-HOB400 gate, HOB200 and HOB400 are used as the lower and upper size gate, respectively. The numbers above the bars indicate the percentage difference in the gated concentration relative to the mean concentration.